Corrosion resistance improvement of iron-yttrium mixtures by powder metallurgy.

William Arnulfo Aperador-Chaparro[1], Irma Inirida Angarita-Moncaleano[2], Mónica Natalia López-Camargo[3]
[1]*Universidad Militar Nueva Granada, Bogota - Colombia,* [2,3]*Universidad Nacional de Colombia, Bogota - Colombia*
ORCID: [1]*0000-0001-9006-0020,* [2]*0000-0002-0473-5093,* [3]*0000-0003-1680-2908*

Abstract— It is manufactured by powder metallurgy mixture of 0%, 1%, 3%, 5%, and 7% by weight of Iron Yttrium Oxide to establish the effect of the ceramic on the metal when exposed to stagnant 3.5% Sodium Chloride solution at room temperature. The samples are tested for structural characterization obtained by X-ray diffraction (XRD). At the same time, the analysis of electrochemical properties has been carried out through the study of polarization curves and electrochemical impedance spectroscopy. After the deterioration test for the different mixtures and the corrosion products, the characterization was identified with XRD. The results obtained include the mechanical alloy and the evidence of adding phases (Yttrium Iron Oxide) and (Yttrium Iron) due to the manufacturing process. The specimens had resistance to corrosion with respect to the increase of the ceramic in the metal due to the formation of the phases generated in the mixture. Nevertheless, the adequate percentage has been determined at 5% since this is the optimum quantity incorporated into the Iron, capable of conferring the properties of protection against corrosion.

Keywords: yttrium oxide, iron, corrosion, powder metallurgy.

I. INTRODUCTION

Powder metallurgy is unique in mixing materials with dissimilar or extremely high melting points that tend to react abruptly with the environment when melted [1]. By controlling grinding variables, it is established that microstructural changes are generated in the powder, known as "mechanical alloying", allowing, through compaction and sintering, to produce alloys of certain elements such as Hf. V. Li. Cs. Ni, W. These elements are not easy to obtain or even impossible to prepare by conventional methods such as electric furnace or induction furnace. An example is the formation of ceramic coatings on metal, such as Al2O3 on Al (for capacitors), Nitrided, and Carbides on Ti, which provide insulating properties unattainable by metal alone. Another example is the thin filaments of ceramic superconductors, which are difficult to fabricate and handle. Still, some success has been achieved by preparing a ductile wire containing the appropriate mixture of metals (Ba, Cu, Y) and subsequently converting it by oxidation into the superconductor YBa2Cu3O7-x. A third example is powder metallurgical composites using elastic modulus transfer as the primary hardening mechanism, including metals reinforced with Boron or SiC fibers and concrete reinforced with Carbon fibers. [2]. This technology allows the synthesis of various equilibrium phases and non-equilibrium alloys, whether solid solutions, intermetallics, quasi-crystals, amorphous alloys such as metallic glasses, and micro and nanostructured materials [3]. The intense search for materials capable of resisting extreme conditions, or providing tools with the longest possible service life, leads to the use of ceramic materials in metals, such as Yttrium Oxide (Y2O3), the central axis of this research [4].

Studies regarding mechanical alloying in the Fe-Al system, in a wide range of compositions, show the formation of Fe-based intermetallic compounds and the crystalline and amorphous transformations due to different stages of the process [5]. The behavior of Yttrium Oxide (Y2O3) in pure Iron (Fe) powder particles prepared by mechanical alloying has revealed Yttrium Oxide dissolved in the Iron matrix, which later reorganizes in portions, generating an adequate homogeneity by grinding for at least 12 hours [6-7]. It has been evidenced that "open" atomic volumes present in the ceramic, concluding that especially vacancies are responsible for producing a metastable phase so that the Yttrium Oxide dissolves in pure Iron [8-9].

The fabrication process of materials with the mixture of Iron and Yttrium Oxide has been limited to the relation of the powder conditioning stage by milling. Several results of the mechanical alloying, the structural changes presented, and their mechanical properties have been revealed [10-11].

The purpose of this article is to analyze the effect of mechanical alloying on pure Iron for concentrations of 0%, 1%, 3%, 5%, and 7% (w/w) of Iron Oxide, obtaining a metallic matrix with oxide dispersion and establishing the interrelation between geometric and physical characteristics of the particles according to the tribological behavior and corrosion resistance of the samples. The results indicate that it is possible to achieve an industrial application.

II. EXPERIMENTAL DEVELOPMENT

The manufacturing process was linked to a previous analysis of the powders' conditioning process, including the material's compaction and later with the sintered compact. The grinding cycle was carried out utilizing the Pulverisette 5 Fritsch Planetary Mill. The processes used are grinding (59 minutes), pause (30 minutes), and reverse (59 minutes), whose reverse parameter makes the grinding more efficient by rotating the vial in the opposite direction and also generates the activation of mechano-chemical energy in the material. The rotation speed of the mill was 250 rpm.

The mixed powder material was processed in a Shimadzu UH-I 500kNI universal testing machine, using a mold that allowed the controlled compaction of the material at 0.5 mm/s and a load of 12000 Kgf. Then, the extraction of the piece was performed without compromising the compact powder or the mold. Subsequently, the sintering process was carried out starting with a heating ramp up to 500 °C in a constant time of 60 minutes, maintaining the temperature for 20 minutes, and the ramp was raised for 40 minutes to reach 1000 °C, holding it for 40 minutes; subsequently, it was left to cool in the furnace.

The morphological characterization was carried out using a Tescan Vega 3SB scanning electron microscope, coupled with a system containing the secondary and backscattered electron techniques; the images collected provide surface morphological and dimensional information of the particles. The mineralogical and structural characterizations of the mixtures were performed by X-ray diffraction experiments, which were carried out in a PANalytical EMPYREAN diffractometer with Co-Kα monochromatic radiation with a wavelength of 1.789 Å, in a Bragg-Brentano geometry, with goniometer in θ/θ configuration, in a 2θ range between 10° and 90°, at a step and step time of 0.02° and 2 seconds, respectively. The characterization was performed by identifying the different crystalline phases present in the materials and comparing the particular diffractions of the spectra obtained with the corresponding spectra in the database (Crystallography Open Database). Additionally, from the Rietveld refinement of a high crystallinity standard, the K factor keeps the configuration by which the crystallinity of the standard used was identified and applies it to the patterns obtained whose new values were adjusted to the presence of the crystalline phases related to the crystallographic information present in the identified phases (characteristic peaks) and the presence of wide range signals that represent the amorphous or short-range order content, existing in the studied samples.

The estimation of the damage that may occur due to the effect of the corrosive fluid was performed with a potentiostat - galvanostat Gamry reference 3000 using the techniques of electrochemical impedance spectroscopy and polarization curves, with the configuration of the reference electrochemical cells - ER (Ag/AgCl), the counter electrode -EA (Platinum wire) and the sample holder -ET with a sample exposure area of 1 cm2, the electrodes are immersed in a solution in a solution of sodium chloride, NaCl at 3.5% w/v, this solution was chosen because it simulates a marine solution, it also corrodes active metals forming the chlorides on the metal. Nyquist plots were obtained by performing frequency sweeps from 0.001 Hz to 500 kHz, using a sinusoidal signal amplitude of 5 mV. The Tafel diagrams were obtained at a sweep speed of 0.125 mV/s in a voltage range from -0.25 V to 0.25 V using an exposed area of 1 cm2. The equipment configuration was carried out considering the guidelines indicated by the ASTM G3, G5, and G59 standards [12, 13]. The degradation phenomena were observed with a scanning electron microscope (SEM). The surface characteristics were determined with a JEOL NeoScope JCM-5000 scanning electron microscope equipped with electronic optics with a magnification range of 50-40000X.

24

Aibi research, management and engineering journal. Volume 9, Number 3, September - December 2021, ISSN 2346-030X PP 23-31.

III.   RESULTS

a.   Scanning electron microscopy

In Figures 1a-1e, the micrographs are observed to determine whether they are based on the direct observation of the particles using the estimation technique through scanning electron microscopy coupled to the Gatan Digital Micrograph software. For analysis, experimental and statistical control, the data are recorded in Table 1, where the descriptive count of the particle size distribution of each of the samples analyzed is generated. The particle behaviors after conditioning are deduced [14].

Figures 1a-1e show the images recorded in the SEM of 0%, 1%, 3%, 5%, and 7%, allowing to perceive aspects of diffusion between particles, showing lower limit for the case of 1 and 3%, consequent to the values of lower porosity, this is a measure of the effectiveness of the diffusion starting from the process of refinement of the particle size, where the material with the smallest particle size with respect to the dispersion of the values quantified in the SEM, is associated with the lowest porosity, also distinguished instantaneous area reduction, the irregular shape was identified after its mechanical obtaining process [15].

The porosity was determined by shades, which can become other types of material such as oxides, under EDS and visual electron microscopy at high magnification found utilizing the backscattered electron detector. It was determined that the dark tone in the intermediate zones of the grains was porosity and did not correspond to material different from the matrix. The porosity defines the effectiveness of diffusion starting from the particle size refinement process, where the material with the smallest particle size with respect to the dispersion of the values quantified in the SEM [15] is found to be associated with the lowest porosity. The samples with Yttrium Oxide content presented lower porosity, with the lowest value related to the percentages of 3, 5, and 7%.

Table 1 shows the data obtained from the software where it is observed as in the SEM images, all systems have a different level of porosity, and the dependence with the median value of the particle size is obtained. This is related to the initial characteristics of the powder, and its percentage ratio of the densified Y2O3 due to the sintering state and the consolidation pressure are similar for all samples [16].
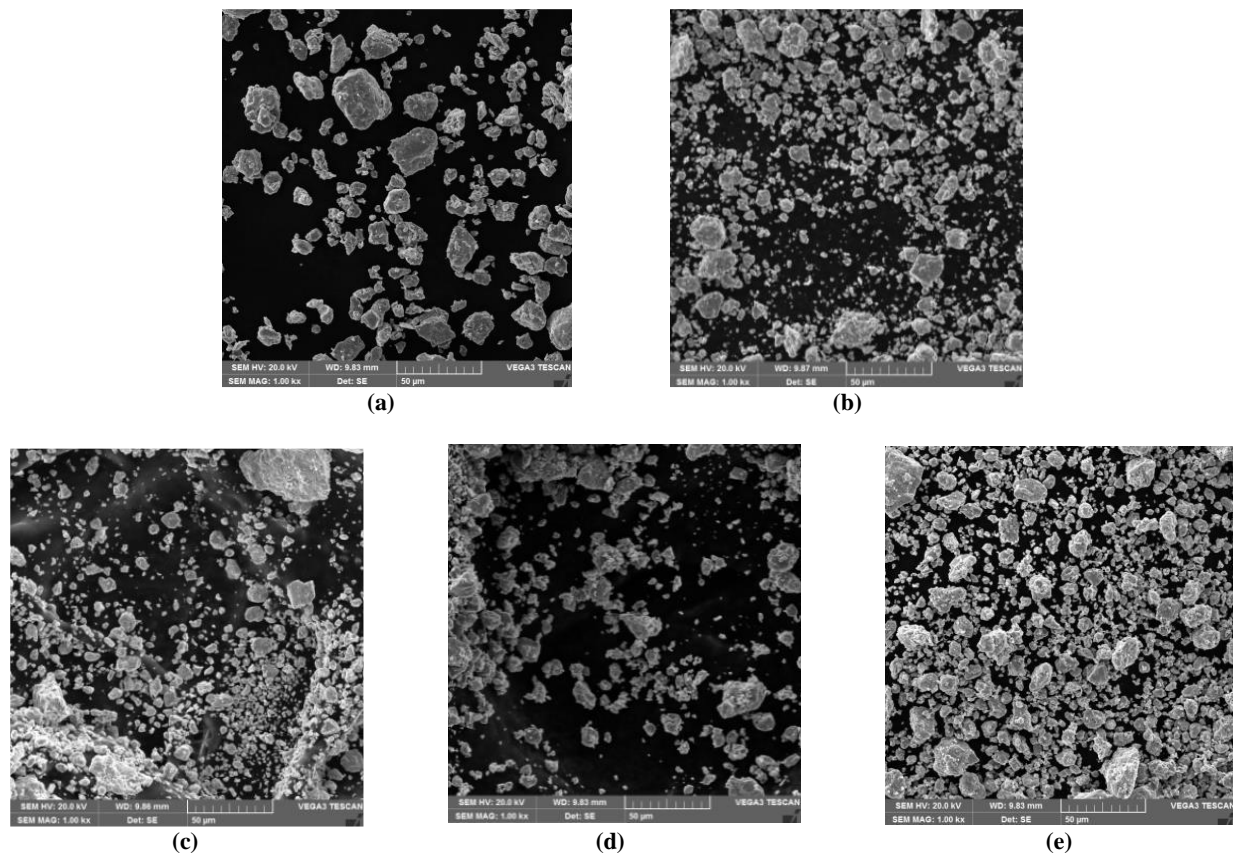

Figure 1: Microscopies of the samples with different percentages of Y_2O_3, a) 0%, b) 1%, c) 3%, d) 5%, e) 7%.
Source: Prepared by the authors.

Table 1: Recording of Gatan Digital Micrograph software data that determines the porosity size and statistics of scanning electron microscopy images.

	Larger size μm^2	Smaller size μm^2	Median
0%	90.37	8.03	30.60
1%	26.17	1.29	6.82
3%	20.88	0.88	7.32
5%	27.68	1.90	7.89
7%	25.18	2.29	8.14

Source: Prepared by the authors.

Figure 2 shows the quantitative SEM elemental analysis generated by energy-dispersive X-ray (EDS) detecting contaminants and proportions of elements [17]. The conditioned material shows a decrease in particle size with respect to the increase in the concentration of Yttrium Oxide in Iron, showing the effectiveness of the selected variables of the process. With the support of the EDS analysis after the conditioning cycle, a homogeneous distribution of Yttrium Oxide particles in the Iron was established. The presence of chromium is generated by the collision of the spheres with the material to be pulverized [18].
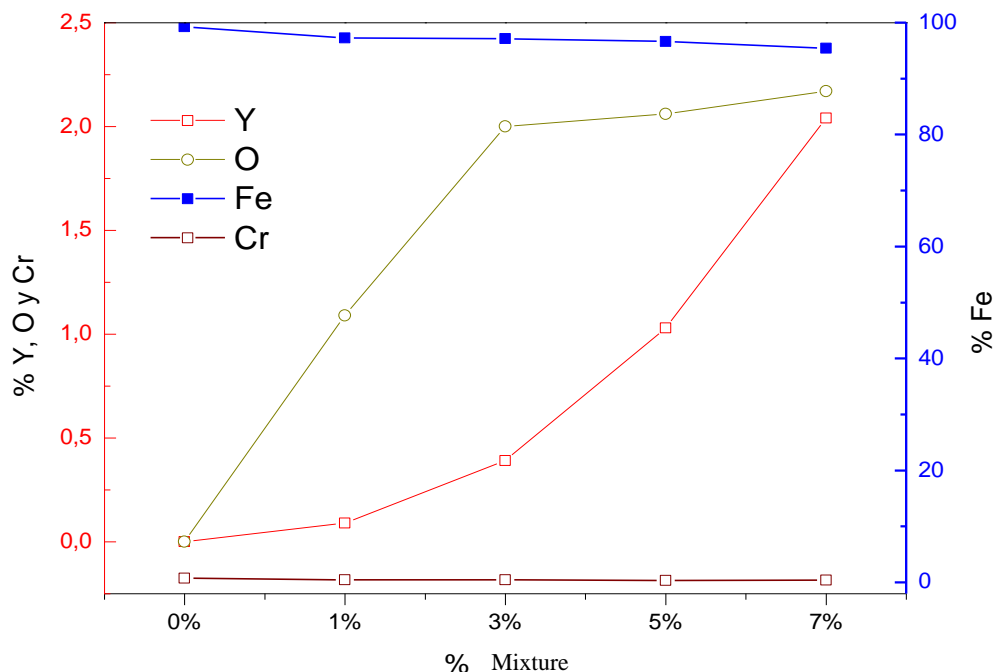

Figure 2: Elemental composition of the samples.
Source: Prepared by the authors.

b. 3.2 X-Ray Diffraction

In Figure 3, the diffraction patterns of Iron without mixture called 0%, and the mixtures of concentration of Yttrium Oxide in Iron (1, 3, 5, and 7%) are obtained, where iron oxides are found because the mixture is not performed under controlled atmosphere, the mechanically conditioned concentrations showed the presence of monoclinic Iron, determined by the software HighScore (Plus), which is integrated into the XRD, presenting a tendency of the diffractogram to maintain a wide peak width, as opposed to those appearing in the position of an angle of 45°, in the samples of 1%, 3%, 5% and 7%, compounds such as FeYO3, Fe5Y3O12 and Y2O3 product of mechanical alloying, is the effect of the formation of new phases due to the energy generated during the process. In the diffractogram of the 0% sample, the concentration of iron oxide corresponding to hematite (65°) and magnetite (82°) that are a consequence of the reactions during the process due to the temperature generated by the collision of the spheres, the vial, the powder, and its respective frequency, as well as the lack of control of the atmosphere inside the mill [19-20].

The higher degree of deformation validates the bonding between the particles and ratifies the effectiveness of the diffusion process in sintering [21-22]. The 5% and 7% systems obtain the highest elongation while the load is applied inside the compaction mold; therefore, the peaks are obtained with greater intensity. For the case of 7%, a peak is observed at 34°, manifesting that the sintering process led the material at such concentrations of yttrium oxide to a better diffusion. The shrinkage of the material after sintering is related to the density of the material, and because the amorphous regions in the spectrum are not observable, likewise the grain size of the material was affected by the density; where the densest samples observed by SEM are 3, 5 and 7% where smaller grain sizes were obtained [23-24].
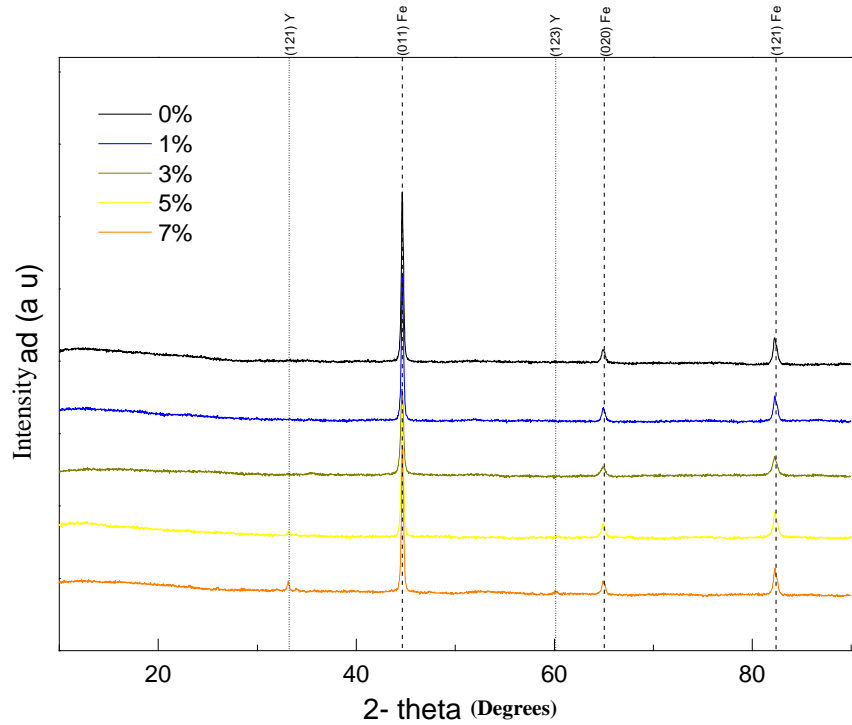
Figure 3: X-ray diffraction spectra on sintered specimens.
Source: Prepared by the authors.

The values in Figure 4 correspond to the species found under the spectrum analysis, where Iron is found for the five samples, as well as percentages of Yttrium Iron Oxide in the samples of 1, 3, 5, and 7% increasing with respect to increasing concentration [25-26].
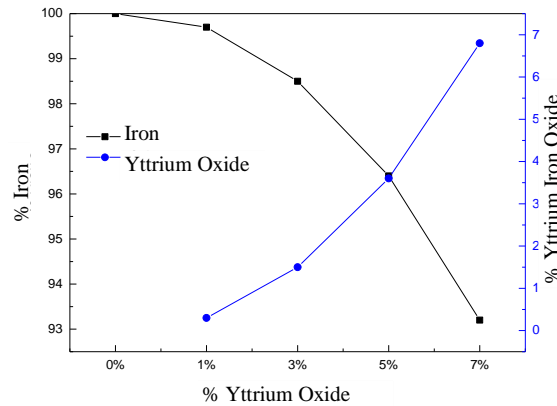

Figure 4: Percentage values of Iron and Y_2O_3.
Source: Prepared by the authors.

c.   3.3 Electrochemical evaluation

From the impedance diagrams in Figure 5, it is observed that the behavior of the Iron matrices with different Y2O3 additions presents a different behavior in each evaluated percentage [27]. The resistance to polarization or resistance to charge transfer for the matrices was calculated with the sum of the resistance of the porous layer and the resistance of the barrier layer. For sample 7% presents resistance to charge transfer has a value of 1.55 Kohm, the resistance to charge transfer of specimens of 5%, 3%, 1%, and 0% presented a decrease compared to 7%, with values of 0.871 Kohm, 0.631 Kohm, 0.216 Kohm, and 0.160 Kohm, respectively, noting that the resistance that opposes the passage of load, in each of the cases may be due to the amount or density of iron material with Y2O3 mixture [28]. The significant variation of resistance to load passage is due to the percentage of oxide, which increases with the mixture. It can be observed that there is a variation in the capacitance of the porous and barrier layers (Cc and Ccorr) as a function of the time used to obtain the parts.

27

Aibi research, management and engineering journal. Volume 9, Number 3, September - December 2021, ISSN 2346-030X PP 23-31.
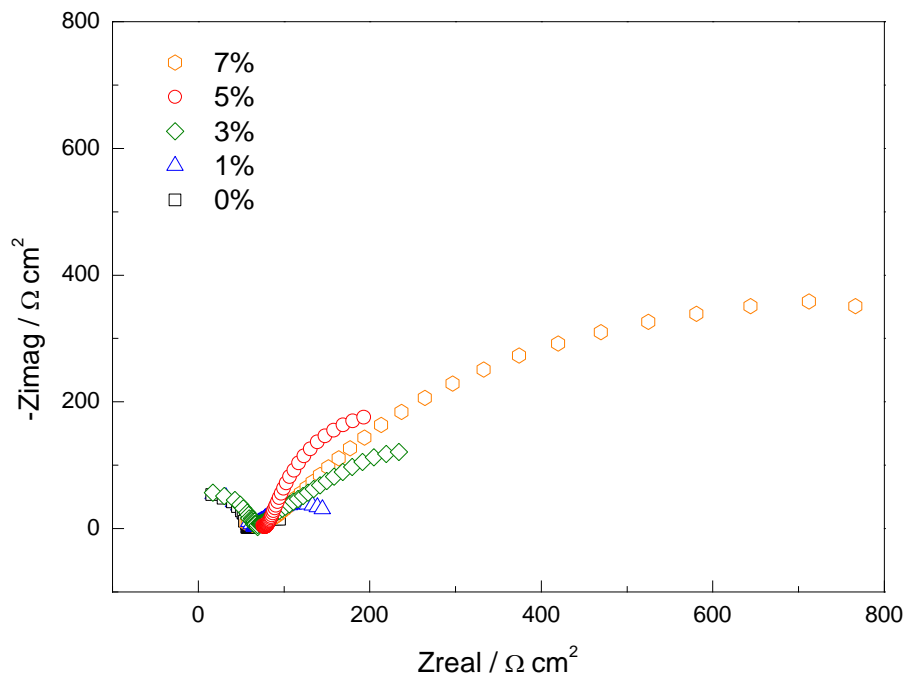
Figure 5: Nyquist plot corresponding to the value of impedance decreases as a function of decreasing Yttrium Oxide percentage.
Source: Prepared by the authors.

The interpretation of the data obtained requires modeling employing an electrical circuit analogous to the physical system studied, also called an equivalent circuit. The model that provided the best fit was presented in Figure 6. The equivalent circuit has two sets of constant phase elements. It is due to a surface oxide layer generated in each of the systems evaluated and with a second porous layer, which can be associated with the porosity present in the materials [29].
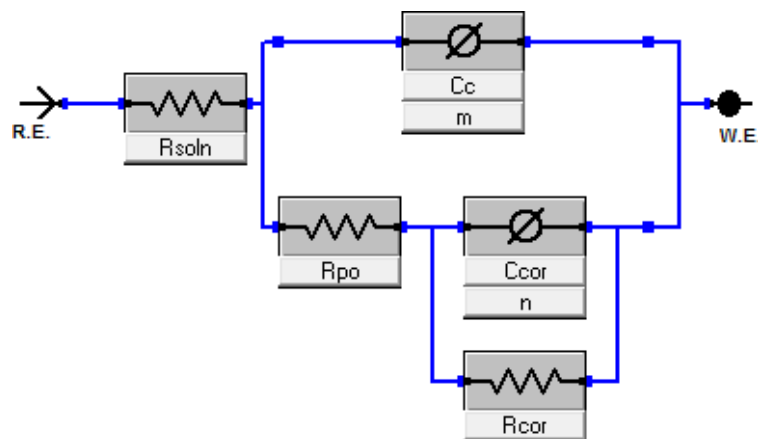

Figure 6: Equivalent circuit corresponding to the evaluation of powder metallurgical specimens with added yttrium oxide.
Source: Prepared by the authors.

The corrosion potentials of the polarization curves in Figure 7, found for each material, are shown in Table 2 (Ecorr). The displacement of the Tafel diagrams toward regions of passivity where the Ecorr is more positive, and this is consistent with the corrosion rate; that is, as the Tafel diagrams move to a zone of protection, it also moves to a zone of lower corrosion rate. This behavior of the study materials is characteristic when evaluating by Tafel slopes the iron alloys with the percentage increase of Yttrium Oxide [30].

Since the Tafel diagrams of the study material move to anodic regions while corroding at a lower rate, it could be due to general corrosion occurring in the study material that generates a gradual increase in corrosion rate [31].

When analyzing the iron matrix reinforced with 5 and 7% of Y2O3, it is obtained that as the number of Y2O3 particles in this matrix increases, the spacing between them decreases, as observed in the SEM images in Figures 1d and 1e, which would lead to the presence of smaller anodic areas propitiating corrosion an additional protection [32]. Added to the fact that the presence of particles in the matrix increases the concentration of crystalline and metallurgical defects, mainly around the particles where corrosion inhibition can be generated in a saline medium, however, it can be determined that 5% is a limiting weight for corrosion protection, since the values are similar, the corrosion kinetics is similar for the contents of 5% and 7%, as observed in Table 2.

William Arnulfo Aperador Chaparro, Irma Inirida Angarita Moncaleano, Mónica Natalia López Camargo
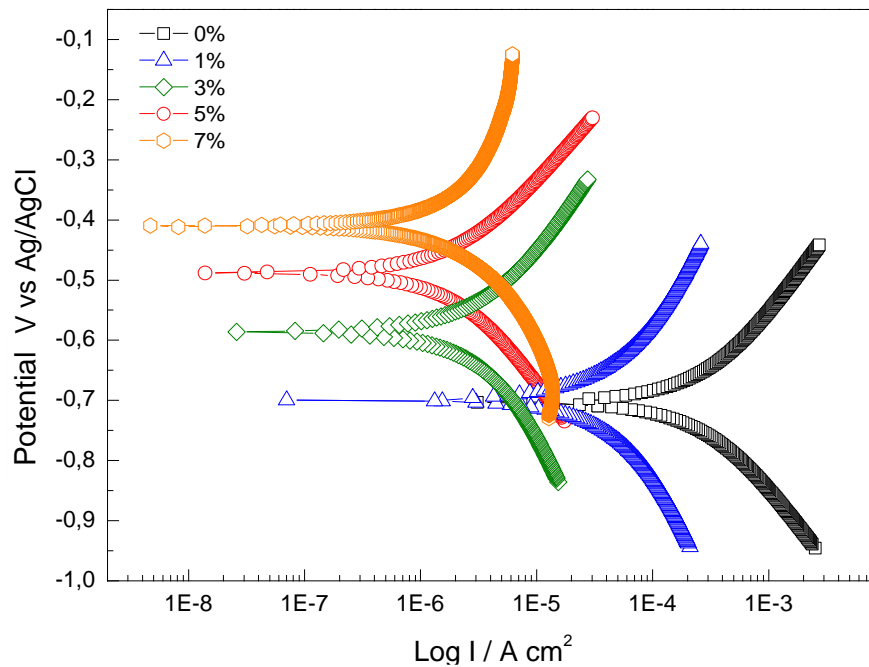
Figure 7: Tafel Polarization Curves for 0%, 1%, 3%, 5%, and 7%.
Source: Prepared by the authors.

Table 2. Data obtained from the Tafel curves by the fitting method

Parameter	0%	1%	3%	5%	7%
Anodic slope V/ decade e^{-3}	270,6	225,4	322,0	459,0	381,0
Cathodic slope V/ década e^{-3}	260,8	273,8	468,0	508,4	243,8
Corrosion potential mV	-703,0	-700,0	-586,0	-490	-406
Corrosion current	302,0	40,1	4,740	1.41	1.29
Corrosion rate mpy	701,7	93.07	11,02	3.27	2.99

Source: Prepared by the authors.

IV. CONCLUSIONS

The conditioned material presented a particle decrease with respect to the increase of the concentration of Yttrium Oxide in Iron, showing the effectiveness of the selected variables of the process. In addition, the EDS analysis after the conditioning cycle established the existence of a homogeneous distribution of Yttrium Oxide particles in the Iron.

With the XRD technique, the values corresponding to the species found after the spectrum analysis were determined. Iron is found in the five samples, and percentages of FeYO3 in the 1, 3, 5, and 7% increase with respect to the rise in concentration. The mechanically conditioned concentrations showed the presence of monoclinic Iron presenting a diffractogram trend, as opposed to the characteristics of alpha iron, which appears at the height of the 45° position. During the analysis, compounds such as FeYO3 were identified in the 1%, 3%, 5%, and 7% samples as a product of the mechanical alloying, which is the effect of the formation of new phases due to the energy generated during the process.

The resistance to polarization or resistance to charge transfer for the 7% samples shows a resistance to charge transfer of higher value; the 5%, 3%, 1%, and 0% specimens showed a decrease with respect to the reduction of Yttrium Oxide content as well as the corrosion rate values given in millimeters per year, which increases according to the increase of the concentration of yttrium oxide in Iron of the sample.

When analyzing the reinforced iron matrix in weight of Y2O3 in the electrochemical tests, it is obtained that as the number of Y2O3 particles increases, the spacing between them should decrease, which would lead to the presence of smaller anodic areas providing additional corrosion protection. Added to this is the fact that the presence of particles in the matrix increases the concentration of crystalline and metallurgical defects, mainly around the particles where corrosion inhibition can be generated in a saline medium. However, it can be determined that 7% is a maximum weight of corrosion protection, but it should be considered that the corrosion kinetics is very similar for contents of 5% and 7%.

V. ACKNOWLEDGMENTS

VI. REFERENCES

[1] A. Elsayed, J. Umeda, K. Kondoh, Effect of quenching media on the properties of TiNi shape memory alloys fabricated by powder metallurgy, Journal of Alloys and Compounds, Volume 842, 2020, 155931, ISSN 0925-8388, https://doi.org/10.1016/j.jallcom.2020.155931.

[2] S. Parvizi, S. Mahdi-Hashemi, F. Asgarinia, M. Nematollahi, M. Elahinia, Effective parameters on the final properties of NiTi-based alloys manufactured by powder metallurgy methods A review, Progress in Materials Science, 2020, 100739, ISSN 0079-6425, https://doi.org/10.1016/j.pmatsci.2020.100739.

[3] S. Raynova, F. Yang, L. Bolzoni, Mechanical behaviour of induction sintered blended elemental powder metallurgy Ti alloys, Materials Science and Engineering A, Volume 799, 2021, 140157, ISSN 0921-5093, https://doi.org/10.1016/j.msea.2020.140157.

[4] K. Maclin, J. Vasanth, P. S. Lokendar-Ram, V. Pon-Anand, M. Prabu, S. Rahul, Experimental investigation of mechanical and tribological properties of Aluminium metal matrix composites fabricated by powder metallurgy route – A review, Materials Today: Proceedings, 2020, ISSN 2214-7853, https://doi.org/10.1016/j.matpr.2020.07.057.

[5] M. F. Stroosnijder, J. D. Sunderkötter, M. J. Cristóbal, H. Jenett, K. Isenbügel, M.A. Baker, The influence of yttrium ion implantation on the oxidation behaviour of powder metallurgically produced chromium, Surface and Coatings Technology, Volume 83, Issues 1–3, 1996, Pages 205-211, ISSN 0257-8972, https://doi.org/10.1016/0257-8972(95)02741-6.

[6] Y. Zhuang, X. Zhang, T. Peng, H. Fan, X. Zhang, Q. Yan, A. A. Volinsky, Effects of yttrium oxides on the microstructure and mechanical properties of 15-15Ti ODS alloy fabricated by casting, Materials Characterization, Volume 162, 2020, 110228, ISSN 1044-5803, https://doi.org/10.1016/j.matchar.2020.110228.

[7] Z. Lv, Y. Wu, J. Dang, D. Liu, L. Hu, K. Du, H. Sun, Effect of yttrium on morphologies and size of tungsten carbide particles prepared through CO reduction, Journal of Materials Research and Technology, Volume 9, Issue 5, 2020, Pages 10166-10174, ISSN 2238-7854, https://doi.org/10.1016/j.jmrt.2020.07.028.

[8] A. P. Shivprasad, S. C. Vogel, V. K. Mehta, M. W. D. Cooper, T. A. Saleh, J. T. White, J. R. Wermer, E. P. Luther, H. R. Trellue, Thermophysical properties of high-density, sintered monoliths of yttrium dihydride in the range 373–773 K, Journal of Alloys and Compounds, Volume 850, 2021, 156303, ISSN 0925-8388, https://doi.org/10.1016/j.jallcom.2020.156303.

[9] Y. Long, J. Che, Z. Wu, H. T. Lin, F. Zhang, High entropy alloy borides prepared by powder metallurgy process and the enhanced fracture toughness by addition of yttrium, Materials Chemistry and Physics, Volume 257, 2021, 123715, ISSN 0254-0584, https://doi.org/10.1016/j.matchemphys.2020.123715.

[10] Z. Xiao, H. Geng, Ch. Sun, P. Jia, H. Luo, Effect of yttrium on properties of copper prepared by powder metallurgy, Advanced Powder Technology, Volume 26, Issue 4, 2015, Pages 1079-1086, ISSN 0921-8831,https://doi.org/10.1016/j.apt.2015.05.003.

[11] K. Chen, J. Peng, C. Srinivasakannan, S. Yin, S. Guo, L. Zhang, Effect of temperature on the preparation of yttrium oxide in microwave field, Journal of Alloys and compounds, Volume 742, 2018, Pages 13-19, ISSN 0925-8388, https://doi.org/10.1016/j.jallcom.2018.01.258.

[12] ASTM G3-14(2019), Standard Practice for Conventions Applicable to Electrochemical Measurements in Corrosion Testing, ASTM International, West Conshohocken, PA, 2019.

[13] ASTM G59-97(2020), Standard Test Method for Conducting Potentiodynamic Polarization Resistance Measurements, ASTM International, West Conshohocken, PA, 2020.

[14] M. Saremi, Z. Valefi, Thermal and mechanical properties of nano-YSZ–Alumina functionally graded coatings deposited by nano-agglomerated powder plasma spraying, Ceramics International, Volume 40, Issue 8, Part B, 2014, Pages 13453-13459,ISSN 0272-8842, https://doi.org/10.1016/j.ceramint.2014.05.068.

[15] K. J. Hwang, M. Shin, Y. Wook-Lee, M. H. Lee, H. Lee, T. H. Shin, Effects of YSZ powder properties on its corrosion behaviour for solid oxide membrane (SOM) electrolysis process, Journal of the European Ceramic Society, Volume 39, Issue 15, 2019, Pages 4864-4873, ISSN 0955-2219, https://doi.org/10.1016/j.jeurceramsoc.2019.06.048.

[16] D. Salehzadeh, P. Marashi, Z. Sadeghian, E. deposited Ni(OH)2-YSZ and NiO-YSZ nanocomposite coatings, microstructural and electrochemical evaluation, Surface and Coatings Technology, Volume 381, 2020, 125155, ISSN 0257-8972, https://doi.org/10.1016/j.surfcoat.2019.125155.

[17] S. Yin, J. Cizek, C. Chen, R. Jenkins, G. O'Donnell, R. Lupoi, Metallurgical bonding between metal matrix and core-shelled reinforcements in cold sprayed composite coating, Scripta Materialia, Volume 177, 2020, Pages 49-53, ISSN 1359-6462, https://doi.org/10.1016/j.scriptamat.2019.09.023.

[18] F. Khodabakhshi, A. Simchi, The role of microstructural features on the electrical resistivity and mechanical properties of powder metallurgy Al-SiC-Al2O3 nanocomposites, Materials & Design, Volume 130, 2017, Pages 26-36, ISSN 0264-1275, https://doi.org/10.1016/j.matdes.2017.05.047.

[19] Z. Deng, H. Yin, C. Zhang, G. Zhang, W. Li, T. Zhang, R. Zhang, X. Jiang, X. Qu, Microstructure and mechanical properties of Cu–12Al–xNi alloy prepared using powder metallurgy, Materials Science and Engineering: A, Volume 759, 2019, Pages 241-251, ISSN 0921-5093, https://doi.org/10.1016/j.msea.2019.05.051.

[20] A. Elsayed, M. Bahlol, A. Zayed, Effect of Ti addition on properties of porous Fe-Ni-Co-Al high entropy alloy manufactured by powder metallurgy, Materials Today: Proceedings, Volume 24, Part 2, 2020, Pages 942-948, ISSN 2214-7853, https://doi.org/10.1016/j.matpr.2020.04.406.

[21] L. Bolzoni, Low-cost Fe-bearing powder metallurgy Ti alloys, Metal Powder Report, Volume 74, Issue 6, 2019, Pages 308-313, ISSN 0026-0657, https://doi.org/10.1016/j.mprp.2019.01.007.

[22] S. Dhar, A. Jena, S. C. Patnaik, S. K. Sahoo, Omkar Tripathy, A study on microstructure and mechanical properties of aluminium matrix composites with micro-sized iron fillers produced by powder metallurgy route, Materials Today: Proceedings, 2020, ISSN 2214-7853, https://doi.org/10.1016/j.matpr.2020.03.733.

[23] W. Li, Q. Hu, Y. Liu, M. Zhang, J. Wang, X. Han, C. Zhong, W. Hu, Y. Deng, Powder metallurgy synthesis of porous Ni-Fe alloy for oxygen evolution reaction and overall water splitting, Journal of Materials Science & Technology, Volume 37, 2020, Pages 154-160, ISSN 1005-0302, https://doi.org/10.1016/j.jmst.2019.06.021.

[24] S. Ehtemam-Haghighi, H. Attar, I. V. Okulov, M. S. Dargusch, D. Kent, Microstructural evolution and mechanical properties of bulk and porous low-cost Ti–Mo–Fe alloys produced by powder metallurgy, Journal of Alloys and Compounds, Volume 853, 2021, 156768, ISSN 0925-8388, https://doi.org/10.1016/j.jallcom.2020.156768.

[25] A. Muhammad, A. Faiz , S. M. Puteri, Y. Noorhana, A. Muhammad, Investigation of boron effect on the densification of Fe-50%Ni soft magnetic alloys produced by powder metallurgy route, Materials Today: Proceedings, Volume 16, Part 4, 2019, Pages 2210-2218, ISSN 2214-7853, https://doi.org/10.1016/j.matpr.2019.06.112.

[26] L. Xiangrong, L. Junbo, J. Xiong, Y. Lu, G. Qingshan, S. Xiangyu, G. Zhixing, H. Tao, L. Mengxia, Wear and corrosion resistant Mn-doped austenitic cast iron prepared by powder metallurgy method, Journal of Materials Research and Technology, Volume 9, Issue 3, 2020, Pages 6376-6385, ISSN 2238-7854, https://doi.org/10.1016/j.jmrt.2020.03.099.

[27] M. Dehestani, K. Trumble, H. Wang, H. Wang, L. A. Stanciu, Effects of microstructure and heat treatment on mechanical properties and corrosion behavior of powder metallurgy derived Fe–30Mn alloy, Materials Science and Engineering: A, Volume 703, 2017, Pages 214-226, ISSN 0921-5093, https://doi.org/10.1016/j.msea.2017.07.054.

[28] C. Jiang, J. Lu, W. Liu, Y. Xing, F. Zhang, Y. Chen, Corrosion resistance of plasma-sprayed Fe-based coatings by using core-shell structure powders, Journal of Materials Research and Technology, Volume 9, Issue 6, 2020, Pages 12273-12280, ISSN 2238-7854, https://doi.org/10.1016/j.jmrt.2020.08.081.

[29] W. Xu, X. Lu, J. Tian, C. Huang, M. Chen, Y. Yan, L. Wang, X. Qu, C. Wen, Microstructure, wear resistance, and corrosion performance of Ti35Zr28Nb alloy fabricated by powder metallurgy for orthopedic applications, Journal of Materials Science & Technology, Volume 41, 2020, Pages 191-198, ISSN 1005-0302, https://doi.org/10.1016/j.jmst.2019.08.041.

[30] N Singh, O. P. Kumar, Phase evolution, mechanical and corrosion behavior of Fe(100-x) Ni(x) alloys synthesized by powder metallurgy, Journal of Physics and Chemistry of Solids, Volume 114, 2018, Pages 8-20, ISSN 0022-3697,https://doi.org/10.1016/j.jpcs.2017.10.045.

[31] W. Aperador, J. C. Caicedo, C. España, G. Cabrera, C. Amaya, Bilayer period effect on corrosion–erosion resistance for [TiN/AlTiN]n multilayered growth on AISI 1045 steel, Journal of Physics and Chemistry of Solids, Volume 71, Issue 12, 2010, Pages 1754-1759, ISSN 0022-3697.

[32] J. Čapek, K. Stehlíková, A. Michalcová, Š. Msallamová, D. Vojtěch, Microstructure, mechanical and corrosion properties of biodegradable powder metallurgical Fe-2 wt% X (X = Pd, Ag and C) alloys, Materials Chemistry and Physics, Volume 181, 2016, Pages 501-511, ISSN 0254-0584, https://doi.org/10.1016/j.matchemphys.2016.06.087.

[33] M. C. Conti, B. Mallia, E. Sinagra, P. Schembri-Wismayer, J. Buhagiar, D. Vella, The effect of alloying elements on the properties of pressed and non-pressed biodegradable Fe–Mn–Ag powder metallurgy alloys, Heliyon, Volume 5, Issue 9, 2019, e02522, ISSN 2405-8440, https://doi.org/10.1016/j.heliyon.2019.e02522.